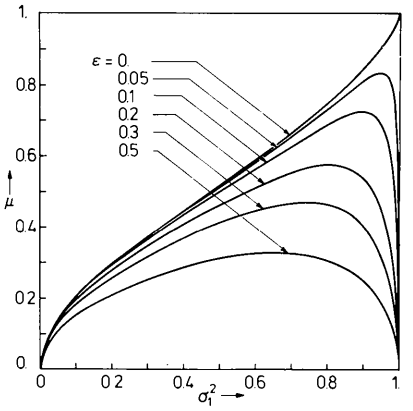

Fig. 4. Signal-to-noise ratio as a function of σ_1^2 for different accuracies of measurement.

with

$$\varepsilon^2 = \langle \sigma_F^2 \rangle / \Sigma_N.$$

Fig. 4 shows the variation of μ as a function of σ_1^2 for different values of the mean normalized error ε. It demonstrates the loss of structural information for finite ε as $\sigma_1^2 \to 1$. There occurs an optimum signal-to-noise ratio for $\sigma_1^2 \simeq 1 - \varepsilon$.

Assume the critical value of μ for the statistical significance of the features in the map to be 0·5 corresponding to $\sigma_1^2 \simeq 0{\cdot}5$ for the error-free data. This implies that data with $\varepsilon = 0{\cdot}1$ should allow a structure completion from inspection of difference maps up to $\sigma_1^2 \simeq 0{\cdot}98$. With $\varepsilon = 0{\cdot}05$ the corresponding value of σ_1^2 is even greater than 0·99. Hence, in general, accuracy of measurement should not be a very critical factor.

A similar result is obtained from another argument. The observed data should meet the condition

$$\langle |F_N - F_P| \rangle > \langle \sigma_F^2 \rangle^{1/2}, \qquad (35)$$

which can be rewritten in terms of the residual $R(F)$ $(=\langle |F_N - F_P| \rangle / \langle F_N \rangle)$ as

$$\frac{\sqrt{\pi}}{2} R(F) > \varepsilon \qquad (36)$$

since $\langle F_N \rangle = (\sqrt{\pi}/2)\Sigma_N^{1/2}$ (Wilson, 1949), Now, using the theoretical expression for $R(F)$ (Srinivasan, Raghupathy Sarma & Ramachandran, 1963) we find, for example, ε $(\sigma_1^2 = 0{\cdot}97) < 0{\cdot}1$ and ε $(\sigma_1^2 = 0{\cdot}99) < 0{\cdot}06$. The case that σ_2^2 is small occurs especially in protein crystallography when difference Fourier maps are used to reveal small molecules added to the protein (Henderson & Moffat, 1971).

Equation (25) implies a preponderance of positive errors, *i.e.* $F_N^o > F_N$. The resulting bias in the density, however, is quite small. The average height of an atomic peak in an $F_N^o \exp(i\varphi_N)$ map is obtained as $(1 + \varepsilon^2)/(1 + 2\varepsilon^2)^{1/2}$ times the true height.

The author is very grateful to Professor H. Dachs for having initiated and supported this work.

References

ABRAMOWITZ, M. & STEGUN, I. A. (1965). *Handbook of Mathematical Functions*, p. 298. New York: Dover.

HENDERSON, R. & MOFFAT, J. K. (1971). *Acta Cryst.* B**27**, 1414–1420.

LIPSON, H. & COCHRAN, W. (1968). *The Determination of Crystal Structures*, p. 223. London: Bell.

LUZZATI, V. (1952). *Acta Cryst.* **5**, 802–810.

LUZATTI, V. (1953). *Acta Cryst.* **6**, 142–152.

NIXON, P. E. & NORTH, A. C. T. (1976). *Acta Cryst.* A**32**, 325–333.

SRINIVASAN, R. & CHANDRASEKARAN, R. (1966). *Indian J. Pure Appl. Phys.* **4**, 178–186.

SRINIVASAN, R. & PARTHASARATHY, S. (1976). *Some Statistical Applications in X-ray Crystallography*. Oxford: Pergamon Press.

SRINIVASAN, R., RAGHUPATHY SARMA, V. & RAMACHANDRAN, G. N. (1963). *Crystallography and Crystal Perfection*, edited by G. N. RAMACHANDRAN. London: Academic Press.

WILSON, A. J. C. (1949). *Acta Cryst.* **2**, 318–321.

Acta Cryst. (1983). A**39**, 761–767

A Varying-Step Algorithm for Numerical Integration of Takagi–Taupin Equations

BY Y. EPELBOIN

Laboratoire de Minéralogie–Cristallographie, associé au CNRS, Université Pierre et Marie Curie, 75230 Paris CEDEX 05, France

(*Received* 13 *September* 1982; *accepted* 3 *May* 1983)

Abstract

The numerical integration of the Takagi–Taupin equations using a constant step of integration does not allow the simulation of traverse topographs since the accuracy of the computation is rather poor. A new algorithm is described in which the step of integration varies inside the crystal, following the oscillations of the amplitudes of the wavefields. The precision becomes good enough to simulate either section topographs, taking into account the real width of the incident beam, or traverse topographs. Moreover in most cases the

0108-7673/83/050761-07$01.50

time of computation is decreased by a factor of two to three.

Introduction

The first numerical integration of the Takagi–Taupin equations was performed by Authier, Malgrange & Tournarie (1968). The method they suggested, the so-called 'half-step derivative method', used in conjunction with a constant step of integration has been very successful. It has been possible to simulate the contrast of dislocations in section topographs (Balibar & Authier, 1967; Epelboin, 1974; Chukovskii, 1974), of planar defects in the Laue–Bragg case (Epelboin, 1979) and of ferromagnetic walls (Nourtier, Kleman, Taupin, Miltat, Labrune & Epelboin, 1979). In the Bragg case, Bedynska, Bubakova & Sourek (1976) simulated the contrast of a screw dislocation perpendicular to the surface; Riglet, Sauvage, Petroff & Epelboin (1980) studied the contrast of a dislocation parallel to the surface of a thin crystal. Bragg-case experiments have been simulated using an incident plane wave: Ishida, Miyamoto & Kohra (1976) compared a plane-wave experiment in the Laue case to its simulation.

The use of a constant-step algorithm (CSA) has been very useful to determine physical parameters of various defects and X-ray topography became a quantitative method for characterizing materials.

Yet many difficulties remain. A rigorous choice of the step of integration is rather delicate. It depends upon diffraction conditions and theoretically each simulation for given reflection conditions would need a long and delicate study to determine the best step of integration: big enough to allow fast calculations and to limit rounding errors, small enough so that the numerical equations do not diverge and do not give false solutions. In practice this study is done once and a given step of integration is used as long as the result seems to be satisfactory. Moreover, it is well known (Epelboin, 1977) that the direct image of a defect is strongly underestimated whenever it exists and no studies of this part of the contrast can be done through simulations. This is because the Takagi–Taupin (TT) equations diverge along the edges of the Borrmann fan: a step of integration which is satisfactory in the middle of the fan becomes too large along the edges and, as explained before, it is not possible to decrease it.

All these limitations do not come from the half-step derivative method itself but from the use of a constant step of integration. Very recently, Nourtier & Taupin (1983) have shown that this method remains the best one for integrating such equations. For a given accuracy it is the fastest and simplest algorithm.

To take into account the divergence of the TT equations, Petrashen (1976) suggested decreasing the step of integration near the edges of the Borrmann fan. But no criterion was given about where to switch from one step to the other and how to choose them. No proof was given that the direct image of a defect became satisfactory.

In this paper we will present a new method of integration of the TT equations based on the half-step derivative method. We will explain how it is possible to let the step of integration vary in all the Borrmann fan and we will compare the accuracy of the varying step algorithm (VSA) with the constant-step algorithm (CSA).

First, we will recall the limitations of the CSA, then we will explain the basic principles of the VSA. In the last part we will show some applications to the study of the contrast of dislocations in X-ray section topographs.

I. Limitations of constant-step algorithms

(a) *The half-step derivative method*

The half-step derivative method has been explained in numerous papers (see, for example, Authier *et al.*, 1968; Epelboin, 1977) and we will just briefly recall its results.

Let $\mathbf{s}_0$ and $\mathbf{s}_h$ be the edges of the Borrmann fan (Fig. 1). This triangle is divided by a network of characteristics parallel to $\mathbf{s}_0$ and $\mathbf{s}_h$, respectively, q is the distance between B and A, p the distance between C and A.

Using the half-step derivative method the TT equations may be transformed into a set of numerical equations where the amplitudes of both reflected and refracted waves at a given point A inside the crystal depend upon the amplitudes of these waves at points B and C only:

$$\begin{bmatrix} D_0(s_0, s_h) \\ D_h(s_0, s_h) \end{bmatrix} = \frac{1}{1-W-AB} \begin{bmatrix} 1-W & A(1-W) & AB & A(1+W) \\ B & AB & B & 1+W \end{bmatrix} \times \begin{bmatrix} D_0(s_0-p, s_h) \\ D_h(s_0-p, s_h) \\ D_0(s_0, s_h-q) \\ D_h(s_0, s_h-q) \end{bmatrix}, \quad (1)$$

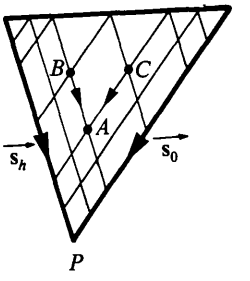

Fig. 1. Principle of integration of the TT equations.

where

$$A = -(i/2)\,\pi p k \chi_{\bar{h}}$$
$$B = -(i/2)\,\pi q k \chi_h$$
$$W = i\pi q\left[k\beta_h - \frac{\partial}{\partial s_h}\,\mathbf{g}.\mathbf{u}\,(s_0, s_h - q/2)\right].$$

χ_h and $\chi_{\bar{h}}$ are the Fourier components of the dielectric susceptibility, $\mathbf{g}$ is the reciprocal-lattice vector for the reflection studied and $\mathbf{u}$ the local deformation of the crystal. $k = 1/\lambda$ and β_h is a parameter which expresses the departure from exact Bragg conditions of the incident wave. In the case of an incident spherical wave it is null.

For the CSA p and q are fixed throughout the crystal, for the VSA they vary from one point to the next.

(*b*) *Criticism of the CSA*

As already mentioned, the choice of the lengths of p and q is delicate. Since the computation time is proportional to the number of knots in the network of integration, *i.e.* to $1/p^2$ and $1/q^2$, p and q must be as large as possible. Their lengths are limited by the order of approximation of the numerical method (see Epelboin, 1977).

But the most critical point is that boundary conditions along the entrance surface and the edges of the Borrmann fan must also be taken into account. We will consider only the case of an incident spherical wave where the boundary conditions along the surface may be simulated by the lightening of one point source only because, as will be explained later, the CSA remains very satisfactory for simulating plane-wave topographs. In the Laue case the amplitude of the wave fields oscillates very rapidly along the edges of the Borrmann fan. To follow these oscillations p and q should be chosen so small that computation time would be tremendously long and that double or quadruple precision would be needed in the computer to avoid numerical errors. Moreover, their values would have to be adapted upon changing any geometrical and diffraction conditions. The values of the lengths of p and q being the result of a compromise explains why the direct image of a defect is underestimated: this image comes from the interaction of the wave fields with the local deformation in a region where the density of knots of the network of integration is not large enough.

In most simulations p and q are of the order of 2 to 3 μm. This means that the distance Δ between B and C (Fig. 1) varies from 0·3 to 2 μm depending upon the values of the Bragg angle. The period of oscillation of the amplitude of the wave fields is of the order of 1 μm near the edges of the Borrmann fan and thus they cannot be taken into account. The time of computation is about 12s using an IBM 370/168 computer for a crystal 800 μm thick. This means that a complete section topograph is simulated in 10 to 50 min depending upon the thickness of the crystal and the height of the image.

Using 1 μm for p and q would multiply the time of computation by a factor of four, which is really unrealistic. In the case of an incident plane wave, the edges of the Borrmann fan are avoided, the incident wave having theoretically an infinite width, thus the CSA remains the best algorithm for simulating any kind of plane-wave topographs, double-crystal or synchrotron radiation experiments.For section topographs these limitations remain reasonable as long as one is interested in the dynamic or intermediary image of a defect but become intolerable for simulating traverse topographs where most of the contrast arises from the integration of the direct image of the defect in the scanning. A detailed discussion and numerical data may be found in Epelboin (1977).

II. Principles of varying-step algorithms

The purpose of the VSA is to find a way to adapt the local steps of integration to the local variations of the amplitudes of the wave fields at any point inside the Borrmann fan. The best idea would be to choose p and q through a trial-and-error method at each step of the calculation, so that the network of integration would always be adapted to the local diffraction conditions, which means that the number of knots would be sufficient to describe the amplitude variations of the waves at any point inside the crystal. This method leads to very complicated algorithms and would require an unreasonable computation time. This means that the network of integration must be known before starting the integration of (1), based on previous knowledge of the diffraction and geometrical conditions.

(*a*) *Choice of the steps along the edges of the Borrmann fan*

Since the TT equations diverge along the edges of the Borrmann fan the steps p and q must be as small as possible near $\mathbf{s}_0$ and $\mathbf{s}_h$. The position of the extinction fringes in a perfect crystal is a good criterion to follow the oscillations of the amplitude of the wave fields. Since analytical solutions exist (Kato, 1961) it is possible to determine the position of these fringes along the exit surface of the crystal. Let $\boldsymbol{\xi}$ be an axis along this surface (Fig. 2). The intensity of the fringes is given by the J_0 Bessel function and the position of their minima may be computed by calculating the zeros of

J_0. For our purpose an asymptotic development is sufficient after the second zero:

$$J_0(\xi) \simeq \left(\frac{4}{2\pi\xi}\right)^{1/2} \cos(\xi - \pi/4). \qquad (2)$$

Knots of the network of integration are placed along ξ so that a reasonable number of points describes the variation of intensity between two zeros along the exit surface. From these points we draw characteristic lines parallel to $\mathbf{s}_0$ and $\mathbf{s}_h$, respectively, and a knot of the network of integration will be positioned at each intersection of two lines. This gives the network shown in Fig. 3. On the edges of the Borrmann fan the steps of integration are small enough to follow the oscillations of the amplitudes of the waves; in the middle the steps increase to rather large values since the amplitude of the wave fields varies slowly.

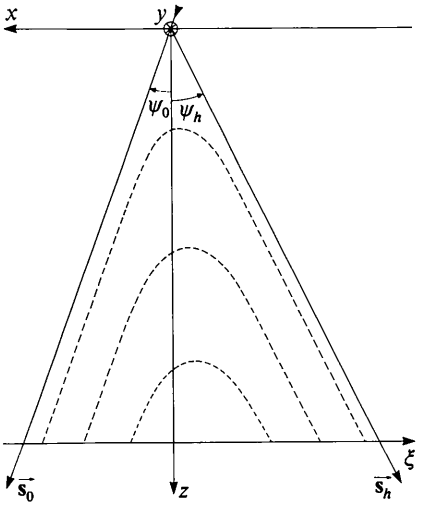

Fig. 2. Geometry of the computation.

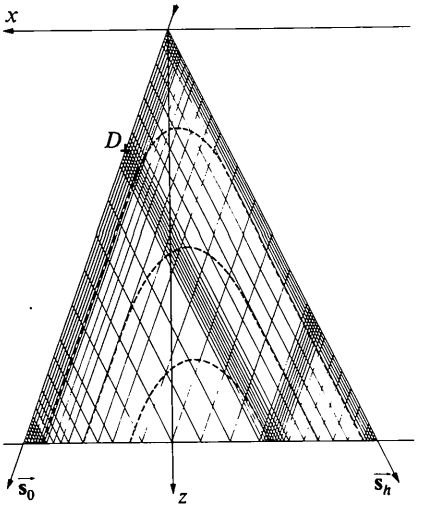

Fig. 3. Principles of the integration network.

The upper and lower limits of the lengths of the steps is a function of the diffraction conditions; let Δ be the distance between two successive points on the axis ξ. We may write:

$$p = \frac{\cos \psi_0}{\sin 2\theta} \Delta$$

$$q = \frac{\cos \psi_h}{\sin 2\theta} \Delta. \qquad (3)$$

We have tried to determine upper and lower values for Δ which would be valid for most cases. We have computed the intensity profile on the exit surface of a perfect crystal for various geometries and various diffraction conditions and come to the following conclusion: a minimum length $\Delta_{min} = 0{\cdot}2$ μm near the edges of the Borrmann fan is satisfactory and a maximum length $\Delta_{max} = 1{\cdot}6$ μm in the central part of the profile also seems to be reasonable. For very high quality simulations it might be necessary to decrease it to 0·8 μm to match the best resolution of photographic plates.

Fig. 4 presents intensity profiles computed using the VSA in (*a*) and the CSA in (*b*). In the first profile we note how the intensity increases near the edges compared to the drastic decrease seen in (*b*). The number of visible fringes is greater in (*a*) and is in agreement with the theoretical profile. Δ varies from 0·2 μm near the edges to 1·6 μm in the central part of the drawing. $\Delta = 0{\cdot}8$ μm in all parts of the image in Fig. 4(*b*). 400 points in the network of integration were necessary to describe the exit surface using the CSA *versus* 238 points using the VSA. At the same time it was possible to obtain greater accuracy and to minimize the calculation.

In different calculations we have tested larger values for Δ_{max} but very quickly the approximation became too large for an accurate result and 1·6 μm seems to be the largest reasonable value for Δ_{max}. On the other hand, a smaller minimum step Δ_{min} does not seem to increase the accuracy of the computation. All these tests have been done for experimental conditions corresponding to a mean extinction distance Λ varying from 20 to 70 μm. Minimum values for Δ should certainly be decreased in the case when $\Lambda/\Delta_{min} < 100$.

(*b*) *Taking into account the direct image of a defect*

The direct image of a defect originates from the distorted areas which intersect the refracted waves propagating along $\mathbf{s}_0$. When the photoelectric absorption is low most of the contrast of the defect comes from the diffraction of these waves. The wave-field amplitudes vary tremendously and the local steps p and q determined in the perfect crystal may become completely inaccurate. It is thus necessary to decrease

their values locally to follow the oscillations of the wave fields in the most distorted parts of the crystal. The problem is to estimate the size and shape of the area where the steps must be modified.

The criterion we have used is based on the theory of the direct image explained by Authier (1967). More recently, Miltat & Bowen (1975) have shown that this simple theory is in rather good agreement with the experiment.

Authier suggested that the contrast of the direct image arises from the areas where the distortion is so great and varies so quickly that kinematic diffraction becomes a valid approximation. The size of this image may be estimated by considering the region where the disorientation of the reflecting planes is greater than the width of the intrinsic rocking curve at half maximum, *i.e.*

$$\delta(\Delta\theta) > \frac{2}{\sin 2\theta}\left(\frac{\gamma_h}{\gamma_0}\right)^{1/2}(\chi_h\chi_{\bar{h}})^{1/2}, \qquad (4)$$

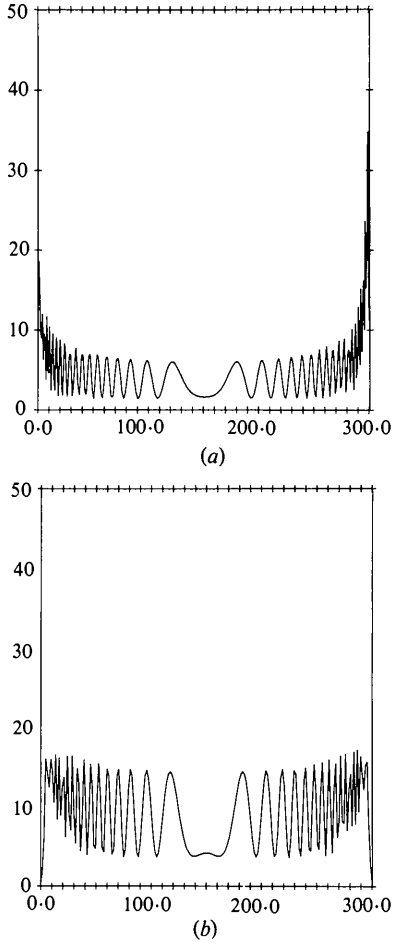

Fig. 4. Profile of the reflected intensity along the exit surface. Mo $K\alpha$, 220 reflection of silicon, 800 μm thick. (*a*) VSA Δ_{min} = 0·2 μm, Δ_{max} = 1·6 μm; (*b*) CSA Δ = 0·8 μm. Intensity units are arbitrary and cannot be compared.

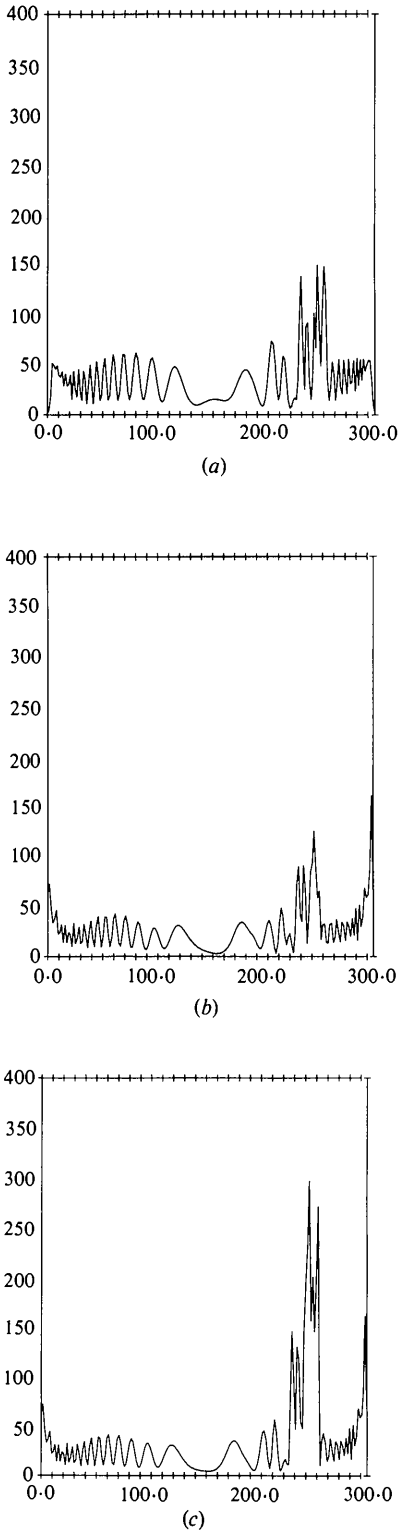

Fig. 5. Profile of the reflected intensity when the direct image of a dislocation exists (see Fig. 6*c*). Same conditions as before. (*a*) CSA Δ = 0·8 μm; (*b*) VSA Δ_{min} = 0·2 μm, Δ_{max} = 1·6 μm without refinement for the direct image; (*c*) VSA. Same as before except in the direct image where Δ = 0·2 μm. Intensities can be compared between (*b*) and (*c*).

where $\gamma_0 = \cos \psi_0$ and $\gamma_h = \cos \psi_h$ (see Fig. 1).

Since the disorientation of the net planes is given by

$$\delta(\Delta\theta) = -\frac{1}{k \sin 2\theta} \frac{\partial}{\partial s_h} \mathbf{g}.\mathbf{u}(\mathbf{r}), \tag{5}$$

we will decrease the steps p and q in the area where

$$\left| \frac{\partial}{\partial s_h} \mathbf{g}.\mathbf{u}(\mathbf{r}) \right| > 2k\alpha \left(\frac{\gamma_h}{\gamma_0} \right)^{1/2} (\chi_h \chi_{\bar{h}})^{1/2}. \tag{6}$$

α is a coefficient introduced to adjust the size of the computed image to the real experiment as suggested by Miltat & Bowen. A value of 1·5 seems reasonable. This leads to the network of integration shown in Fig. 3. The stems p and q are minimum along the edges of the Borrmann fan then increase in the middle of the triangle. Locally the steps are set to their minimum values in the area where the direct image is formed.

Since the interaction of a defect with the wave fields weakens near $\mathbf{s}_h$ (Epelboin, 1975) it is not necessary to decrease the steps in the right part of the fan to values as small as near $\mathbf{s}_0$. This reduces the number of knots and thus the computation time without degrading the accuracy. Our tests show that a minimum value for $\Delta =$ 0·8 μm is sufficient near $\mathbf{s}_h$, except along the $\mathbf{s}_h$ edge itself where it must come back to the minimum value 0·2 μm. Fig. 5 shows an intensity profile computed in a net plane where the direct image exists for the dislocation shown in Fig. 6(*c*). Fig. 5(*a*) has been calculated using the CSA showing, as explained before, the dramatic intensity drop along the edges. Fig. 5(*b*) is computed using the VSA without refinement for the direct image. In both Figs. 5(*a*) and (*b*) this image appears as a series of sharp peaks and its intensity is roughly of the same order (the curves cannot be directly compared since the normalization is different). Fig. 5(*c*) shows the same profile with refinement of the computation for the direct image. The intensity of the peaks is dramatically increased. This is more in agreement with measured densities of greys in various experiments, where the saturation of the photographic emulsion may be reached.

III. Simulation of section topographs

Fig. 5(*c*) shows the great advantage of taking into account the direct image of a defect but this is unnecessary in the planes of incidence where this image does not exist. To simulate section topographs we will thus use two different networks: one without refinement for the direct image when it does not exist, another in a limited number of planes where the direct image is formed (Fig. 3).

To decrease the time of computation we usually compute one plane of incidence in three, the two missing ones in between being interpolated. This might become visible near the direct image where the intensity varies too quickly and in this region it may be necessary to compute all the planes of incidence. In fact, it depends if one is interested in the direct image itself or in other parts of the contrast. Fig. 6(*a*) is the simulation of a section topograph in a silicon crystal already computed using the VSA as a CSA (Epelboin, 1974). Fig. 6(*b*) takes into account the real width of the incident beam falling on the crystal. Its extension is of the order of 10 μm and the simulation has been obtained by adding five different simulations moving the point source along the entrance surface. The high quality of this simulation, compared to the experiment (Fig. 6*c*) shows the accuracy of the VSA. Moreover, the computation itself was done in half the time needed for the CSA algorithms.

Conclusion

The VSA should replace the CSA in the simulation of any section topograph, *i.e.* when the incident beam is a

(*a*) (*b*) (*c*)

Fig. 6. Section topographs for a dislocation $\mathbf{b} = 1/2\,[110]$. See Epelboin (1974). Diffraction conditions as before. (*a*) One point source. (*b*) Addition of five simulations corresponding to an entrance slit of 10 μm. (*c*) Corresponding topograph.

spherical wave. It enables faster calculations with much higher accuracy.

This becomes absolutely necessary when one is interested in the study of the direct image. As will be explained in another paper, it permits the real width of the X-ray beam incident on the crystal to be taken into account and one may now obtain simulations of very high quality.

We can already announce that the VSA is accurate enough to allow the simulation of traverse topographs. The work is in progress and the first results are very satisfactory.

Most of the tests were done at the IBM J. J. Watson Research Center in Yorktown Heights during time spent as a 'World Trade Scientist Visitor'.

I would like to thank A. Soyer for the final debugging of the corresponding simulation program.

References

AUTHIER, A. (1967). *Adv. X-ray. Anal.* **10**, 9–31.
AUTHIER, A., MALGRANGE, C. & TOURNARIE, M. (1968). *Acta Cryst.* A**24**, 126–136.
BALIBAR, F. & AUTHIER, A. (1967). *Phys. Status Solidi*, **21**, 413–422.
BEDYNSKA, T., BUBAKOVA, R. & SOUREK, Z. (1976). *Phys. Status Solidi A*, **36**, 509–515.
CHUKOVSKII, T. N. (1974). Proc. 2nd ECM, Kesthely, Hungary.
EPELBOIN, Y. (1974). *J. Appl. Cryst.* **7**, 372–377.
EPELBOIN, Y. (1975). *Acta Cryst.* A**31**, 591–599.
EPELBOIN, Y. (1977). *Acta Cryst.* A**33**, 758–767.
EPELBOIN, Y. (1979). *J. Appl. Phys.* **50**, 1312–1317.
ISHIDA, H., MIYAMOTO, N. & KOHRA, K. (1976). *J. Appl. Cryst.* **9**, 240–241.
KATO, N. (1961). *Acta Cryst.* **14**, 627–635.
MILTAT, J. & BOWEN, D. K. (1975). *J. Appl. Cryst.* **8**, 657–669.
NOURTIER, C., KLEMAN, M., TAUPIN, D., MILTAT, J., LABRUNE, M. & EPELBOIN, Y. (1979). *J. Appl. Phys.* **50**, 2143–2145.
NOURTIER, C. & TAUPIN, D. (1983). In preparation.
PETRASHEN, P. V. (1976). *Fiz. Tverd. Tela (Leningrad)*, **18**, 3729–3731.
RIGLET, P., SAUVAGE, M., PETROFF, J. F. & EPELBOIN, Y. (1980). *Philos. Mag.* A**3**, 339–358.

Acta Cryst. (1983). A**39**, 767–772

Theoretical Study of the Influence of the Width of the Entrance Slit on the Contrast of Dislocations in X-ray Topography by Means of Simulations

BY Y. EPELBOIN AND A. AUTHIER

Laboratoire de Minéralogie–Cristallographie, associé au CNRS, Université P. et M. Curie and Paris VII, 75230 Paris CEDEX 05, France

(*Received* 18 *January* 1983; *accepted* 10 *May* 1983)

Abstract

Experimental topographs may be simulated by addition of simulations where one point source is lit on the surface of the crystal. The accuracy of a varying-step integration of Takagi equations is good enough to allow such computations. It is shown that all parts of the contrast are sensitive to the width of the entrance slit and that accurate characterization of defects must take this parameter into account.

Introduction

X-ray topography (Lang, 1959) is a very useful tool for studying the perfection of crystalline materials. The most widely used method, translation topography, allows the characterization of a large volume of the crystal in a single experiment.

Section topography allows a much more precise study of the defects but the experiment is rather delicate and only a small volume of the material is characterized in one experiment. The quality of the experimental setting, especially the width and parallelism of the entrance slit of the camera, become very important and these parameters should be taken into account in all theoretical and experimental studies. Usually the width of the entrance slit, limiting the incoming beam falling on the crystal, is of the order of 10 μm in section topographs and may be increased to values of the order of 100 μm or more in traverse topography.

It is well known that the quality and number of extinction fringes visible in a section topograph depend not only on the perfection of the crystal but also on the accuracy of the setting and on the width of the incoming beam. The narrower the slit is, the greater will be the number of observable fringes. Of course this is limited by the intensity of the X-ray beam!

0108-7673/83/050767-06$01.50